Nanoscale

Cite this: *Nanoscale*, 2012, **4**, 3237

www.rsc.org/nanoscale

PAPER

Thermal fingerprint of silica encapsulated phase change nanoparticles

Chaoming Wang,[ab] Yan Hong,[ab] Minghui Zhang,[ac] Mainul Hossain,[ad] Yang Luo[ae] and Ming Su*[abc]

Received 11th January 2012, Accepted 6th March 2012
DOI: 10.1039/c2nr30092c

This paper describes a new type of silica microspheres that contain a panel of phase change nanoparticles (Field's alloy, indium, tin or lead–tin eutectic alloy). The thermophysical properties of solid–liquid phase change nanoparticles, *i.e.*, composition-dependent melting temperatures, sharp melting peaks, and large thermal scan range, allow construction of a large number of silica microspheres that have thermally distinguishable patterns of melting temperatures.

1. Background

The small size of nanoparticles makes it possible to build ultra-high capacity labeling systems for object identification and biosensing, where unique nanoparticle properties such as optical, magnetic, electric and electrochemical properties are used for readout.[1–10] But the use of nanoparticles to label each object within a large group of objects is limited due to the lack of nanoparticle-specific signature or low labeling capacity of existing methods. The size-dependent optical properties of semiconducting nanoparticles and metallic nanoparticles have broad emission and absorption peaks in the ultraviolet-visible region, which limits types of optically distinguishable nanoparticles with a peak width at half height of 150 nm in 400–900 nm to only a few.[11–14] In the case that metal nanoparticles are used to enhance intensities of Raman scattering signals where sharp peaks exist over a large range, the available Raman active dyes are limited and quantitative signals are hard to obtain.[15,16] In addition, there is no nanoparticle-specific magnetic or electrochemical property, which means that nanoparticles cannot be distinguished from each other based on their magnetic or electrochemical property.

Despite much research on electric, optical, magnetic or chemical property of nanoparticles,[17–21] and encapsulation of nanoparticles inside silica shells, carbon shells, and aluminium matrix,[22–27] the thermodynamic properties of solid metallic nanoparticles have not been studied extensively in the past.[28–35] Especially, there are even fewer studies on the potential use of thermodynamic properties of these nanoparticles.[36–40] Solid state materials exhibit composition dependent solid–liquid phase change at certain temperatures. During phase change, a solid will absorb heat without temperature rise until all the solid is molten, according to the Gibbs phase rule. If the dimension of the solid is small enough that transition time can be negligible, a sharp melting peak will appear during a linear thermal scan, where extra heating power is required to melt the solid to maintain a constant temperature rise. Compared with other solid materials (organic materials, ceramics or salts), metals and alloys have large volumetric latent heats of fusion, and are stable over a large temperature range. Although only a small number of metals in the periodic table can be used due to availability and safety issues, eutectic alloys with sharp melting peaks can be formed, which go directly from solid to liquid phase without pasty stage. Alloys can be designed according to phase diagrams gained in the past or computational thermodynamics. At last, metal nanoparticles with sharp melting peaks have melting peaks distributed over a large temperature range and each type of nanoparticle could be distinguishable from others from their melting point.

This paper describes the design and synthesis of phase change nanoparticles (metals and eutectic alloys), their encapsulation in silica microspheres and their use in biomarker detection (Fig. 1). Eutectic alloys of two or three metals and sharp melting points are designed and made to form nanoparticles. These nanoparticles are larger than critical size (20 nm), and thus will melt at the same temperature as their bulk counterparts. The melting temperature depends on the atomic number of the metal or composition of alloy; and the fusion enthalpy depends on mass and latent heat of fusion. A panel of phase change nanoparticles has been selected and embedded in silica microsphere. The composition-dependent melting point and sharp melting peak of phase change nanoparticles allow creation of a large number of silica microspheres that have a distinguishable pattern of melting temperatures.

According to combination law, if any two of three metals form binary eutectic alloys, these three metals can form one ternary eutectic alloy, and three binary eutectic alloys; and the total number of metals and alloys is seven. For a given number of

[a]*NanoScience Technology Center, University of Central Florida, FL, 32826, USA. E-mail: mingsu@mail.ucf.edu*
[b]*Mechanical, Materials and Aerospace Engineering, University of Central Florida, FL, 32826, USA*
[c]*Key Laboratory of Advanced Energy Materials Chemistry (MOE), College of Chemistry, Nankai University, Tianjin, 300071, China*
[d]*School of Electrical Engineering and Computer Science, University of Central Florida, Orlando, FL, 32826, USA*
[e]*Department of Laboratory Medicine, Southwest Hospital, Third Military Medical University, Chongqing, 400038, China*

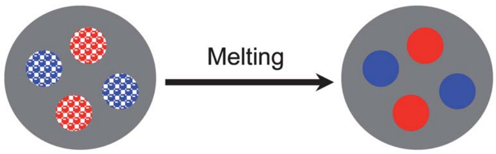

0	1	1	0
1	1 1	2	1
2	1 2 1	4	3
3	1 3 3 1	8	7
4	1 4 6 4 1	16	15
5	1 5 10 10 5 1	32	31
6	1 6 15 20 15 6 1	64	63
7	1 7 21 35 35 21 7 1	128	127
8	1 8 28 56 70 56 28 8 1	256	255
9	1 9 36 84 126 126 84 36 9 1	512	511
10	1 10 45 120 210 252 210 120 45 10 1	1024	1023
n		2^n	2^n-1

Fig. 1 Phase change nanoparticles encapsulated in a silica shell; Pascal's triangle and the number of possible combinations enabled by phase change nanoparticles.

metals that form binary eutectic alloys among any two of them, the numbers of binary alloy, ternary alloy and so on can be derived graphically from Yang Hui's triangle (1238–1298) or Pascal's triangle (1653). The total number of pure metals and eutectic alloys will be

$$\sum_{k=1}^{n} C_n^k - 1 = \sum_{k=1}^{n} \frac{n!}{k!(n-k)!} - 1 = 2^n - 1 \qquad (1)$$

where n is the total number of metals and k is the number of metals in one nanoparticle. 10 different metals that form binary eutectic alloys among any two of them have been found in the periodic table: aluminium, bismuth, cadmium, copper, gadillium, indium, lead, magnesium, palladium, and silver, which can form 10 types of metal nanoparticles, 45 types of binary alloy nanoparticles, 120 types of ternary eutectic alloy nanoparticles, 210 types of quaternary eutectic alloy nanoparticles, and so on. The total number of metals and eutectic alloys is 1023 (see Fig. 1). Note that the combination corresponding to no metal (n is 0) is removed.

2. Experimental

2.1 Materials and chemicals

Organometallic precursors (indium acetate, lead acetate, and tin acetate), indium powder, polyvinylpyrrolidone (PVP, molecular weight of 11 000 Da) and ethylene glycol are from Aldrich. Disuccinimidyl suberate (DSS), *N*-succinimidyl(4-iodo-acetyl) aminobenzoate (SIAB) and tris(2-carboxyethyl) phosphine (TCEP) are from ThermoFisher Scientific (Rockford, IL). Anhydrous dimethyl sulfoxide (DMSO), ammonium hydroxide, anhydrous ethanol, acetone, aminopropyltriethoxysilane (APTES) and tris(hydroxymethyl)-aminomethane (TE) are obtained from VWR (West Chester, PA). Phosphate buffer saline, bovine serum albumin (BSA) and Tween-20 are obtained from Sigma. Field's alloy that contains 32.5% bismuth, 51% indium and 16.5% tin by weight is from Roto Metal Inc. (San Leandro, CA). All chemicals in this study are of analytical grade and used without purification. Immunoreagents are dissolved in pH 7.4 phosphate saline (PBS) buffer (0.01 M in phosphate, 0.14 M NaCl and 2.7 mM KCl) unless otherwise noted. Ultrapure water (18.2 MΩ cm^{-1}) from a Nanopure System (Barnstead, Kirkland, WA) is used.

2.2 Nanoparticle synthesis

Tin nanoparticles are prepared by thermal decomposition of tin acetate: 1 mmol tin acetate is added in 20 ml ethylene glycol with 0.2 g PVP. After heating at 200 °C with magnetic stirring for 20 min, the solution is quenched in 0 °C ethanol (200 ml). The same method is used to make lead nanoparticles. In order to make lead–tin eutectic nanoparticles, 0.37 mmol lead acetate and 0.67 mmol tin acetate are added in 20 ml ethylene glycol with 0.2 g PVP. The mixture is heated to 200 °C while stirring to decompose precursors in nitrogen atmosphere. After reacting for 20 min, the mixture is quenched in 0 °C ethanol. The nanoparticles are separated by centrifuging at 4000 rpm for 10 min, and washing thoroughly with ethanol for three times. Nanoparticles of indium and Field's alloy are prepared by using the nano-emulsion method, where bulk metal or alloy is heated above its melting point in high boiling point poly-α-olefin (PAO) at 200 °C with magnetic stirring in nitrogen atmosphere. After reaction, the nanoparticles are centrifuged, washed with acetone, and checked by transmission electron microscopy (TEM, JEOL 1011), X-ray fluorescence (XRF) spectrometry, and differential scanning calorimetry (DSC). TEM samples are prepared by dispersing a drop of nanoparticle suspension on carbon films supported on copper grids. DSC is done with a PerkinElmer DSC 7, where a sample of 10 mg is hermetically sealed in an aluminium pan and placed inside a DSC chamber under continuously purged nitrogen gas at a heating rate of 10 °C min^{-1} from room temperature to desired high temperatures.

2.3 Encapsulation of phase change nanoparticles

A panel of selected nanoparticles with compositions of Field's alloy, indium, tin, or lead–tin eutectic alloy are embedded in silica microsphere as follows. A silica sol is formed by adding 0.7 ml of tetraethoxysilane (TEOS) and 0.3 ml of 0.05 M HCl in water with ultrasonic stirring for 10 min. An aqueous solution of phase change nanoparticles is added with the final concentration in the range of 5–20% (v). The solution is then mixed with the silica sol, followed by adding 8 ml toluene containing 320 μl Tween-20 and 80 μl Span 80. The volume ratio of organic phase to silica sol is 8 : 1. 1.2 ml of 1% ammonia hydroxide solution is added quickly, which leads to formation of silica microspheres. These microspheres are washed thoroughly with ethanol and water, dried, and checked by DSC, XRF, and scanning electron microscopy (SEM). The compositions are derived with XRF spectrum using a Mini X-ray tube (Amptek Inc., Beford, MA) operating at 40 kV and a tube current of 100 μA and a solid state detector (Amptek Inc., Beford, MA). A Zeiss (Ultra 55) scanning electron microscope (SEM) operated at 5 kV is used to image the morphology of the nanoparticles.

2.4 DNA detection

Oligonucleotides (single stranded DNA, ssDNA) are custom-made at Integrated DNA Technologies Inc. (Coralville, IA). The sequences of oligonucleotides are: capture ssDNA (5′-/5 AmMC6/ATTATTATTATGTGGTTGCTGTGT-3′), target ssDNA (3′-TACACCAACGACACAAATGTTATTAGG-5′), and probe ssDNA (5′-TTACAATAATC-CATTATTATTA/3 Thio-MC3-D-3′). Silica microspheres are modified with amine-terminated monolayers by incubating with 5% (v) APTES in toluene for 3 h at room temperature and washed with toluene and DMSO for three times, respectively. To conjugate probe ssDNA on microspheres, the amine groups at microspheres are incubated with 1 mM SIAB in DMSO for 1 h; disulfide containing probe ssDNA is reduced to 3′ thiolated probe ssDNA by incubating with 0.25 M TCEP at pH 4.5 in TE buffer at 37 °C for 20 min. After removing excess SIAB by washing and centrifugation, microspheres are incubated with the 3′ thiolated probe ssDNA in PBS (pH 8.0) for 3 h. The aluminium substrate is modified with APTES in vapor phase, where the surface is kept in a vial that contains 0.1 ml of APTES and heated for 3 h at 100 °C. The aluminium substrate is then immersed into 1 mM DSS in DMSO solution for 1 h, washed with PBS, and incubated with capture ssDNA in PBS solution (pH 8.0) for 3 h. Probe ssDNA modified silica microspheres and capture ssDNA modified aluminium substrate are added in a TE buffer that contains target ssDNAs for hybridization. After hybridizing for 3 h, the aluminium substrate is taken out of the buffer solution, washed by phosphate buffer and dried for thermal readout. DSC is used to determine the melting point and fusion enthalpy of immobilized silica encapsulated phase change nanoparticles using an empty aluminium pan as reference. The DSC baselines are flattened using Origin software to remove slope and noise after collection.

3. Results and discussions

3.1 Design and synthesis of phase change nanoparticles

The melting temperature of solid nanoparticles depends on their size. When the sizes of nanoparticles are smaller than 20 nm, the surface atoms contribute more in reducing melting temperature. But, the melting temperature is exponentially dependent on size, which makes it difficult or impossible to control melting temperature by controlling nanoparticle sizes, because a small size variation will cause a large deviation of melting temperature. Larger nanoparticles with diameter over 20 nm melt at the same melting temperatures as their bulk counterparts. Fig. 2A and B show two DSC curves of synthesized 30 nm indium and 100 nm tin nanoparticles, which melt at 156 and 231 °C, respectively. Fig. 2C shows the phase diagram of a lead–tin binary alloy derived from CALPHAD (Calculation of Phase Diagram) using Pandat software. The Gibbs free energies of liquid, face-centered-cubic (FCC) and body-centered tetragonal (BCT) are derived at 150, 183 and 350 °C. At 150 °C, the stable phases are FCC and BCT and the liquid phase does not exist; at 183 °C, a tangent line connects the minimum of three phases, indicating a eutectic isothermal; at 350 °C, the only stable phase is liquid. Fig. 2D shows the DSC curve of as-synthesized tin–lead eutectic nanoparticles, which melt at 182 °C, close to the calculated

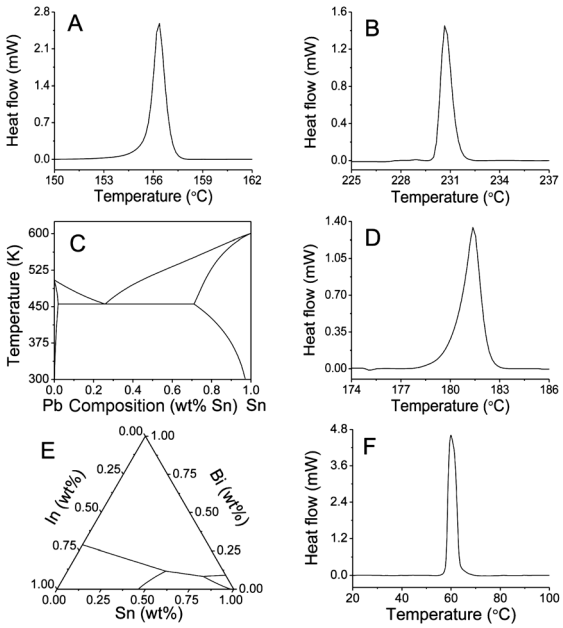

Fig. 2 DSC curves of synthesized indium nanoparticles (A), and tin nanoparticles (B); phase diagram of binary lead–tin alloy (C) and the DSC curve of lead–tin eutectic alloy nanoparticles (D); phase diagram of ternary indium–bismuth–tin alloy (E) and the DSC curve of indium–bismuth–tin eutectic alloy nanoparticles (F).

melting point (183 °C). Similarly, the phase diagram of a ternary alloy of indium, bismuth and tin (Field's alloy) has also been calculated (Fig. 2E), and the DSC curve (Fig. 2F) shows that the alloy nanoparticles melt at 60 °C, which is close to the calculated value of 62 °C. The coincidence of calculated value and experimental value suggests that phase change alloy nanoparticles can be designed to have a pre-defined melting temperature using computational thermodynamics.

3.2 Thermal barcode with phase change nanoparticles

Fig. 3A and B show TEM images of indium and Field's alloy nanoparticles, whose diameters are around 30 and 25 nm, respectively. These nanoparticles can be dispersed in water. Fig. 3C shows the SEM image of silica microspheres that contain indium and tin nanoparticles, and deposited onto a silicon substrate from solution, where the average size of silica particles is about 10 μm. TEM images of large silica particles do not show contrast because electron beams cannot pass through the particles. The composition of silica microspheres is derived by XRF (Fig. 3D), where $L_{\alpha 1}$, $K_{\alpha 1}$ and $K_{\alpha 2}$ of indium at 3.29, 24.21, and 27.27 keV, and $K_{\alpha 1}$ of tin at 25.27 keV can be seen clearly, confirming successful encapsulation of phase change nanoparticles.

The melting temperatures of nanoparticles of Field's alloy, indium, lead–tin eutectic alloy and tin are 62, 156, 183 and 232 °C, respectively. The melting enthalpies (peak areas) are proportional to mass and latent heat of fusion of nanoparticles. The number of thermal probes formed by four types of nanoparticles is 15. Fig. 4 shows the DSC curves collected from 16 different types of silica microspheres, where each curve is flattened to remove slopes and smoothed to remove thermal

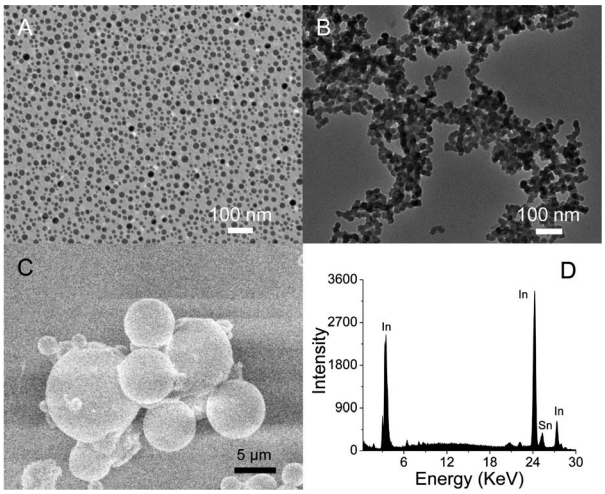

Fig. 3 TEM image of indium (A) and Field's alloy (B) nanoparticles; SEM image (C) and XRF spectrum (D) of silica encapsulated indium and tin nanoparticles.

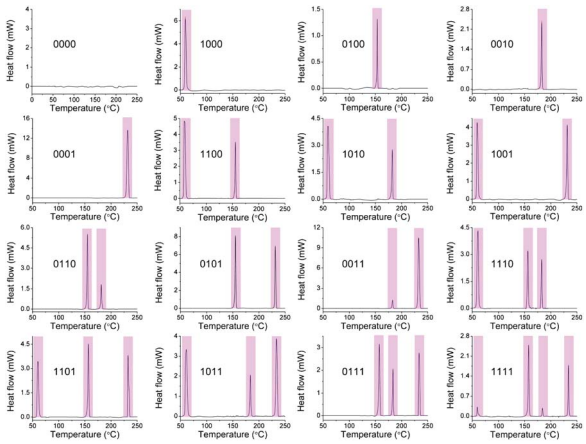

Fig. 4 A panel of DSC curves collected from a series of silica microspheres that contain different ratios of nanoparticles of Field's metal, indium, lead–tin, and tin at melting points of 62, 156, 183, and 231 °C, respectively.

fluctuations. Each melting peak can be denoted as one or zero depending on whether there is detectable heat flux or not. 16 combinations of four elements are 0000, 1000, 0100, 0010, 0001, 1100, 1010, 1001, 0110, 0101, 0011, 1110, 1101, 1011, 0111, and 1111. The height (or area) of each peak corresponds to the amount of certain particles in microspheres. The information in each microsphere can be decoded by counting melting peaks in the DSC curve. One scan from 0 to 300 °C at a ramp rate of 10 °C min^{-1} takes 30 min, and the decoding time can be reduced substantially by increasing ramp rates.

3.3 DNA detection

Target ssDNAs dissolved in PBS (pH 8.0) are detected using silica microspheres that contain nanoparticles of indium and Field's alloy. The probe ssDNA modified microspheres and capture ssDNA modified aluminium pan are added into a buffer solution for hybridization. After hybridizing for 3 h, the aluminium pan is taken out, washed by PBS and tested by DSC. The samples contain a variety of concentrations of target ssDNAs from 100 nM to 1 nM in 1 M NaCl and TE buffer. The melting peaks of nanoparticles are used for qualitative and quantitative detection. Fig. 5A shows the melting peaks of indium and Field's alloy nanoparticles that are encapsulated in silica microspheres, where the curves from top to bottom correspond to target ssDNA concentrations from 100 to 1 nM, respectively. The area of the melting peak is derived by integrating heat flow over the melting range, from which the amount of target ssDNA is derived. Fig. 5B shows the relation between the peak area and the target DNA concentration, where a linear relation exists between concentration and peak area of Field's alloy and indium nanoparticles. The lowest detectable limit is determined to be 1 nM. The sensitivity of the thermal detection method is comparable with optical, magnetic, and fluorescent nanoparticle-based DNA detections.[41–43] It is expected that the thermal detection method can be applied in biomedical and biological fields.

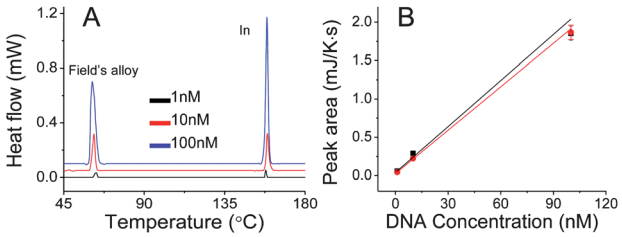

Fig. 5 DSC curves after detecting different concentrations of ssDNA (1 nM, 10 nM and 100 nM) with silica microspheres containing nanoparticles of Field's alloy and indium (A), the peak areas of Field's alloy nanoparticles (square) and indium nanoparticles (circle) *versus* DNA concentration (B).

4. Conclusions

High capacity labeling probes have been made by embedding a panel of phase change nanoparticles inside silica microspheres. Nanoparticles of pure metals, binary and ternary eutectic alloys have been designed according to computational thermodynamics, and prepared by using colloidal methods. These nanoparticles have shown sharp melting peaks at discrete temperatures over a large range. The phase change behaviors of nanoparticles have been confirmed by thermal measurement. The silica microspheres have also been used to detect single strand DNA.

Acknowledgements

This work is supported by a CAREER award from National Science Foundations and a Concept award from Department of Defense. Some characterization works are performed at Materials Characterization Facilities of University of Central Florida.

Notes and references

1 J. Gunn, S. I. Park, O. Veiseh, O. W. Press and M. Zhang, *Mol. BioSyst.*, 2011, **7**, 742.
2 S. Santra, P. Zhang, K. M. Wang, R. Tapec and W. H. Tan, *Anal. Chem.*, 2001, **73**, 4988.

3 A. Biswas, T. Wang and A. S. Biris, *Nanoscale*, 2010, **2**, 1560.
4 C. W. Lu, Y. Hung, J. K. Hsiao, M. Yao, T. H. Chung, Y. S. Lin, S. H. Wu, S. C. Hsu, H. M. Liu, C. Y. Mou, C. S. Yang, D. M. Huang and Y. C. Chen, *Nano Lett.*, 2007, **7**, 149.
5 R. Banerjee, Y. Katsenovich, L. Lagos, M. McIintosh, X. Zhang and C. Z. Li, *Curr. Med. Chem.*, 2010, **17**, 3120.
6 C. Wilhelm and F. Gazeau, *Biomaterials*, 2008, **29**, 3161.
7 S. J. Park, T. A. Taton and C. A. Mirkin, *Science*, 2002, **295**, 1503.
8 M. Rochelet-Dequaire, B. Limoges and P. Brossier, *Analyst*, 2006, **131**, 923.
9 J. Peng, L. N. Feng, Z. J. Ren, L. P. Jiang and J. J. Zhu, *Small*, 2011, **7**, 2921.
10 X. R. Zhang, H. R. Su, S. Bi, S. G. Li and S. S. Zhang, *Biosens. Bioelectron.*, 2009, **24**, 2730.
11 X. Gao, Y. Cui, R. M. Levenson, L. W. K. Chung and S. Nie, *Nat. Biotechnol.*, 2004, **22**, 969.
12 J. Wilcoxon, *J. Phys. Chem. B*, 2009, **113**, 2647.
13 Y. Ohfuti and K. Cho, *J. Lumin.*, 1996, **70**, 203.
14 Y. Williams, A. Sukhanova, M. Nowostawska, A. M. Davies, S. Mitchell, V. Oleinikov, Y. Gun'ko, I. Nabiev, D. Kelleher and Y. Volkov, *Small*, 2009, **5**, 2581.
15 F. S. Manciu, Y. Sahoo, F. Carreto and P. N. Prasad, *J. Raman Spectrosc.*, 2008, **39**, 1135.
16 R. R. Prabhu and M. A. Khadar, *Bull. Mater. Sci.*, 2008, **31**, 511.
17 K. L. Kelly, E. Coronado, L. L. Zhao and G. C. Schatz, *J. Phys. Chem. B*, 2002, **107**, 668.
18 G. Schmid and U. Simon, *Chem. Commun.*, 2005, 697.
19 A. H. Lu, E. L. Salabas and F. Schüth, *Angew. Chem., Int. Ed.*, 2007, **46**, 1222.
20 M. Valden, X. Lai and D. W. Goodman, *Science*, 1998, **281**, 1647.
21 C. J. Ho and J. Y. Gao, *Int. Commun. Heat Mass Transfer*, 2009, **36**, 467.
22 W. Wang and S. A. Asher, *J. Am. Chem. Soc.*, 2001, **123**, 12528.
23 S. Tang, S. Vongehr and X. Meng, *J. Phys. Chem. C*, 2009, **114**, 977.
24 S. Tang, S. Vongehr and X. Meng, *J. Mater. Chem.*, 2010, **20**, 5436.
25 S. Tang, S. Vongehr, Z. Zheng, H. Liu and X. Meng, *J. Phys. Chem. C*, 2010, **114**, 18338.
26 O. G. Tovmachenko, C. Graf, D. J. Van den Heuvel, A. Van Blaaderen and H. C. Gerritsen, *Adv. Mater.*, 2006, **18**, 91.
27 H. W. Sheng, G. Ren, L. M. Peng, Z. Q. Hu and K. Lu, *J. Mater. Res.*, 1997, **12**, 119.
28 Q. Jiang, N. Aya and F. G. Shi, *Appl. Phys. A: Mater. Sci. Process.*, 1997, **64**, 627.
29 K. Morishige and K. Kawano, *J. Phys. Chem. B*, 1999, **103**, 7906.
30 A. N. Goldstein, *Appl. Phys. A: Mater. Sci. Process.*, 1996, **62**, 33.
31 K. Chattopadhyay and R. Goswami, *Prog. Mater. Sci.*, 1997, **42**, 287.
32 F. Ruffino, M. G. Grimaldi, F. Giannazzo, F. Roccaforte and V. Raineri, *Nanoscale Res. Lett.*, 2008, **3**, 454.
33 W. H. Qi, M. P. Wang, M. Zhou and W. Y. Hu, *J. Phys. D: Appl. Phys.*, 2005, **38**, 1429.
34 W. H. Qi, M. P. Wang and G. Y. Xu, *Chem. Phys. Lett.*, 2003, **372**, 632.
35 W. H. Qi and M. P. Wang, *Phys. B*, 2003, **334**, 432.
36 J. Hu, Y. Hong, C. Muratore, M. Su and A. A. Voevodin, *Nanoscale*, 2011, **3**, 3700.
37 M. Zhang, Y. Hong, S. Ding, J. Hu, Y. Fan, A. A. Voevodin and M. Su, *Nanoscale*, 2010, **2**, 2040.
38 Y. Hong, W. Wu, J. Hu, M. Zhang, A. A. Voevodin, L. Chow and M. Su, *Chem. Phys. Lett.*, 2011, **504**, 180.
39 L. Ma, C. Wang, Y. Hong, M. Zhang and M. Su, *Anal. Chem.*, 2010, **82**, 1186.
40 C. Wang, L. Ma, L. Chen, K. Chai and M. Su, *Anal. Chem.*, 2010, **82**, 1838.
41 R. Elghanian, J. J. Storhoff, R. C. Mucic, R. L. Letsinger and C. A. Mirkin, *Science*, 1997, **22**, 1078.
42 D. Gerion, F. Q. Chen, B. Kannan, A. H. Fu, W. J. Parak, D. J. Chen, A. Majumdar and A. P. Alivisatos, *Anal. Chem.*, 2003, **75**, 4766.
43 W. M. Hassena, C. Chaixa, A. Abdelghanib, F. Bessueillea, D. Leonarda and N. Jaffrezic-Renaulta, *Sens. Actuators, B*, 2008, **134**, 755.